Amorphous solid dispersions in poly(ε-caprolactone)/xanthohumol bioactive blends: physicochemical and mechanical characterization

Oroitz Sanchez-Aguinagalde, Emilio Meaurio, Ainhoa Lejardi, Jose-Ramon Sarasua

Published in:
Journal of Materials Chemistry B, Materials for biology and medicine

DOI:
10.1039/D0TB02964E

Publication date:
2021

Document version:
Author Accepted Manuscript (AAM)

Citation for published version (APA):
Oroitz Sánchez-Aguinagalde, Meaurio, E., Ainhoa Lejardi, & Sarasua, J.-R. (2021). Amorphous solid dispersions in poly(ε-caprolactone)/xanthohumol bioactive blends: physicochemical and mechanical characterization. *Journal of Materials Chemistry B*, *9*(20), 4219–4229. https://doi.org/10.1039/d0tb02964e

Amorphous solid dispersions in Poly(ε-caprolactone)/Xanthohumol bioactive blends: physicochemical and mechanical characterization.

Oroitz Sanchez-Aguinagalde, Emilio Meaurio*, Ainhoa Lejardi, Jose-Ramon Sarasua

Department of Mining-Metallurgy Engineering and Materials Science, POLYMAT, University of The Basque Country (UPV/EHU), School of Engineering I, Plaza Ingeniero Torres Quevedo 1, Bilbao, Spain.

* Corresponding author. Fax: +34-94-601-3930

Email: emiliano.meaurio@ehu.eus (E. Meaurio)

Abstract

This paper reports the obtention of amorphous solid dispersions (ASDs) of Xanthohumol (XH) into PCL containing up to 50 wt% of the bioactive compound in amorphous form thanks to the advantageous specific interactions stablished in this system. The miscibility of the PCL/XH blends was investigated using DSC. The melting point depression analysis yielded a negative interaction parameter indicating the occurrence of favorable inter-association interactions. XRD analyses performed at room temperature agree with the crystallinity results obtained on the heating runs performed by DSC. FTIR spectroscopy reveals strong C=O···O-H specific interactions between the hydroxyl groups of XH and the carbonyl groups of PCL. The AFM analysis of the blends obtained by spin-coating shows the variation of crystalline morphology with composition. Finally, tensile tests reveal high toughness retention for the blends in which XH can be dispersed in amorphous form (containing up to 50 wt% XH). In summary, PCL is a convenient matrix to disperse XH in amorphous form, bringing the possibility to obtain completely amorphous bioactive materials suitable for the development of non-stiff biomedical devices.

Keywords: poly(ε-caprolactone) (PCL); Xanthohumol (XH); amorphous solid dispersions (ASDs); interactions; morphology; mechanical properties.

1. Introduction

The successful therapeutic use of medical devices can be compromised by the risk of bacterial infection, that usually begin through biofilm formation. Biofouling is an undesirable process by which harmful microorganisms and their subproducts attach to surfaces, producing extracellular polymers that facilitate adhesion and provide a structural matrix, the so-called biofilm. These biofilms represent a huge risk for public health, as they are responsible for several device-related infections caused by gram-positive or gram-negative bacteria composed biofilms on indwelling medical devices, such as prosthetic heart valves, central venous catheters or urinary catheters, among others [1]–[3]. According to EPINE (Study of the prevalence of nosocomial infections in Spain), urinary infections caused by urinary catheters represent 20.8% of the total nosocomial infections, while vascular catheterization associated bacteremias represent 15.9% [4]. According to World Health Organization (WHO), 8.7% of hospitalized patients present nosocomial infections [5]. Furthermore, biofilms are highly resistant to antibiotic treatment. Antibiotic therapies can reverse symptoms caused by biofilms, but the sessile population of the biofilm remains, having to remove it surgically from the body. This causes a need for removal of any foreign-body material, in addition to long-term, high-dose antibiotic therapies [6]–[8].

Mimicking the defense mechanisms present in nature has been proposed to prevent bioaccumulation, inhibiting both adhesion and growth of microorganisms [9]–[13]. Within this strategy, the antifouling mechanisms of many plant species have aroused great interest, paying attention to the flavonoids that are obtained from their extracts and essential oils. Flavonoids are part of the defense of plants against external aggressions, and works in which their antifouling properties are investigated have been published recently [14]–[18]. In recent years, the interest in Xanthohumol (XH), a natural polyphenol obtained from *Humulus lupulus* has received growing attention due to its wide spectrum of biological activities with beneficial effects on human health [19]. According to recent studies, it presents anti-inflammatory, antioxidant or anticancer properties, among others [19]–[25]. In addition, Xanthohumol displays a broad spectrum of anti-infective activities against different bacteria, such as *Staphylococcus aureus* and *Streptococcus mutans,* with a powerful anti-adherent and antibiofilm activity [26], [27].

Xanthohumol has been reported to inhibit the growth of the Gram-positive bacteria *Staphylococcus aureus* (with a minimal inhibitory concentration MIC of 17.7 μM) and *Streptococcus mutans* (with MIC of 35.3 μM) [28]. Antiviral activity of xanthohumol, in combination with interferon α-2b, was demonstrated against the virus that causes bovine diarrhea (bovine viral diarrhea virus, BVDV E2), which shows considerable similarities with the human hepatitis C virus, and against herpes virus (herpes simplex virus HSV 1 and HSV 2), cytomegalovirus (CMV) and rhinovirus [29]. The xanthohumol concentrations required for antiviral activity (IC_{50}) were in a range of 4.2-7.6 μM. Wang et al. investigated the activity of xanthohumol to suppress several crucial steps in the replication of HIV-1 to treat AIDS patients [30]. A recent review on the antiinfective properties of hop constituents, describes xanthohumol as a broad spectrum anti-infective agent against Gram-positive bacteria, several viruses, fungi (*trichophyton spp.*) and malarial protozoa (*plasmodium falciparum*) [28]. The mechanism/s of the observed inhibitory activities are still under investigation. However, no influence has been reported on Gram-negative bacteria (e.g. *Escherichia coli*) or the *Candida albicans* fungus [31].

Xanthohumol is a prenylated chalcone, a subclass of the flavonoids family [25]. Flavonoids are sparingly soluble compounds, making difficult their obtention and handling [32]. In particular, the solubility reported for xanthohumol in common organic solvents is about 10 mg/ml in ethanol and 35 mg/ml in DMSO (approx. 1 and 3.5 wt% respectively) [33], [34]. This low solubility could be related to comparatively larger intermolecular crystal forces than in other compounds [35]. A priori, compounds poorly soluble in organic solvents are not good candidates to obtain miscible blends with polymeric materials, since increasing the molecular size decreases the favorable entropic contribution to miscibility. But, on the other hand, polymer matrixes can delay the crystallization process of amorphous drugs in the metastable region of the binary phase diagram, increasing the composition range available to obtain useful ASDs [36]–[38]. Using polymers with high glass transition temperatures may further favor ASD obtention due to the vitrification of the system upon cooling [38]; but this property may hardly allow extending the composition range to the unstable region of the miscibility diagram because glassy systems also evolve with time and the unstable amorphous drug will tend to crystalize [39], [40]. Consequently, miscibility is considered a key requisite to obtain stable enough ASDs for practical applications [41]. Unfortunately, polymer-drug

interactions cannot be currently accurately predicted, hence obtaining ASDs is nowadays a trial and error effort [42]. Hence, the number of formulations containing drug in the amorphous form that have made it through to the market is limited due to the generally poor physical stability of the amorphous form [39]. This reveals the need of attention in this research area, particularly considering that about 50% of the new molecules discovered are estimated to have solubility problems [41].

In addition, due to its non-polar, highly hydrophobic nature, XH is nearly insoluble in water. Dispensing the drug in the form of an amorphous solid dispersion (ASD) is usually a good strategy to improve its bioavailability [43], [44]. In this paper, poly (ε-caprolactone) (PCL) has been selected as a suitable matrix to disperse Xanthohumol in the amorphous form based on the hypothesis of the occurrence of favorable hydrogen bonding interactions between the OH groups of XH and the C=O groups in PCL (see scheme 1). PCL is a biodegradable semicrystalline polyester, with glass transition temperature located at about -60° C, and melting point at about 60° C. This polymer is suitable for long-term biomedical applications, as the degradation can last from several months to years [45].

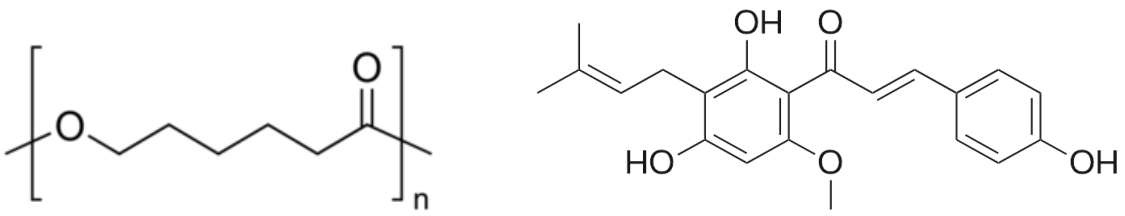

Poly(ε-caprolactone) Xanthohumol

Scheme 1. Chemical structures of PCL and XH.

2. Experimental Section

2.1. Starting Materials

Poly(ε-caprolactone) (PURASORB® PC12 trade name) with an average molecular weight (M_w) of $1.3 \cdot 10^5$ g mol^{-1} and M_w/M_n = 1.76 was purchased from Purac

Biochem (The Netherlands). Xanthohumol (purity 98%) was obtained from Chengdu Biopurify Phytochemicals (China) and tetrahydrofuran (THF) was supplied by Labkem.

2.2 Blend Preparation

Films were prepared by solvent casting at room temperature from tetrahydrofuran (THF) solutions containing 2.5 wt% of PCL/XH blend.

2.3. Differential Scanning Calorimetry (DSC)

Thermal analyses were conducted on a Modulated DSC Q200 from TA Instruments. All the scans were carried out in hermetic aluminum pans under nitrogen atmosphere with sample weights between 5 and 10 mg. In order to study the glass transition temperatures, two consecutive scans were performed with a scan rate of 20°C/min: the first one from -90°C to 130°C to ensure complete melting of the polymeric phase and the second one from -90°C to 300°C. In the case of neat XH, the sample was heated up to 175ºC during the first scan in order to be able to observe the glass transition heat jump during the consecutive DSC scan with minimal sample degradation. The glass transition temperatures (T_g) were measured in the second scan as the midpoint of the specific heat increment.

2.4. Melting Point Depression

The melting point depression of XH was analyzed in XH-rich blends containing 0-20% PCL. To obtain the melting temperature of XH crystals, samples were heated in the DSC with a scan rate of 1°C/min. Three samples were measured for each composition. No weight loss was observed during the thermal treatments.

2.5. Fourier Transform Infrared Spectroscopy (FTIR)

A Nicolet AVATAR 370 Fourier transform infrared spectrophotometer was used to record FTIR spectra of the blends, averaged over 64 scans in the 400-4000 cm^{-1} range with a resolution of 2 cm^{-1}. Tetrahydrofuran solutions containing 2 wt% PCL/XH blend were cast on KBr pellets by evaporation of the solvent at room temperature. Traces of tetrahydrofuran were removed placing the films into a heated vacuum oven for 24 h. The absorbance of the samples was within the range where Lambert-Beer law is obeyed. Second derivative spectra were smoothed using the Norris-Williams Gap Derivatives [ref] using maximum gap sizes and segment lengths of 5 points and 5 cm^{-1} respectively in the derivative transformations.

2.6. Atomic Force Spectroscopy (AFM)

Atomic Force Microscopy was performed using a Nanoscope V controller multimode AFM (Veeco, Santa Barbara, USA). The images were recorded in tapping

mode between 0.2 and 2 Hz. Silicon tip on nitride lever cantilevers of 0.4 N m^{-1} with reflective aluminum back sides (Bruker AXS, Santa Barbara, USA) were used. The image processing was performed using the Nanoscope 9.2 program (Bruker AXS, Santa Barbara, USA).

2.7. X-ray Diffraction (XRD)

To collect the X-ray diffraction patterns a Philips X'pert PRO automatic diffractometer was used, operating at 40 kV and 40 mA, in theta-theta configuration, secondary monochromator with Cu-Kα radiation (λ = 1.5418 Å) and a PIXcel solid state detector (active length in 2θ 3.347°). Data were collected from 4 to 70° 2θ (step size 0.026 and time per step = 72.42 s) at room temperature. A fixed divergence and antiscattering slit giving a constant volume of sample illumination was used.

2.8. Tensile tests

Tensile tests were carried out in an Instron 5565 universal testing machine at a crosshead displacement rate of 5 mm/min at room temperature. Specimens 60 mm length and 10 mm wide were cut from films of 80 μm average thickness. Young's modulus (E), yield stress (σ_y) and strain at break (ε_b) were determined as the mean value of at least four determinations. Data were subjected to one-way analysis of variant (ANOVA) with the level of significance set at $p < 0.05$.

2.9. In Vitro Release Studies (UV-Vis)

UV–Vis absorption spectra were recorded using a Perkin Elmer Lamda 265 UV-Visible spectrophotometer. Before performing the drug release experiments, a calibration curve was obtained measuring the absorbance at a wavelength of 370 nm for solutions of xanthohumol in 0.1 M PBS (pH 7.4) with concentrations ranging from 1 to 15 ppm. Three PCL/XH systems containing 2, 5 and 10 wt% XH were measured in triplicate using samples of about 3 mg (containing about 60, 150 and 300 μg XH) obtained by solvent casting. Samples were immersed in 4 ml of 0.1 M PBS buffer at 37º C. At fixed time intervals of 15 min., the whole solution was replaced with fresh one, and the solution taken out was used to measure the drug concentration by UV spectroscopy using the calibration curve.

3. Results and Discussion

3.1. Miscibility analysis by DSC according to single glass transition criterion.

When two components are miscible, the blend is expected to show a single glass transition temperature (T_g) located between the T_gs of the neat materials, which is expected to change progressively with composition [46], [47]. On the contrary, more than one single value could be detected if there is a separation into individual amorphous phases within the system. Figure 1 shows the second scan DSC traces for PCL, XH and their blends. As can be seen, the glass transition temperature of pure XH is located at about 71°C, while the T_g of pure PCL occurs at about -62° C. All the PCL/XH blends show single intermediate glass transition temperatures, indicating miscibility in the amorphous phase in the whole composition range.

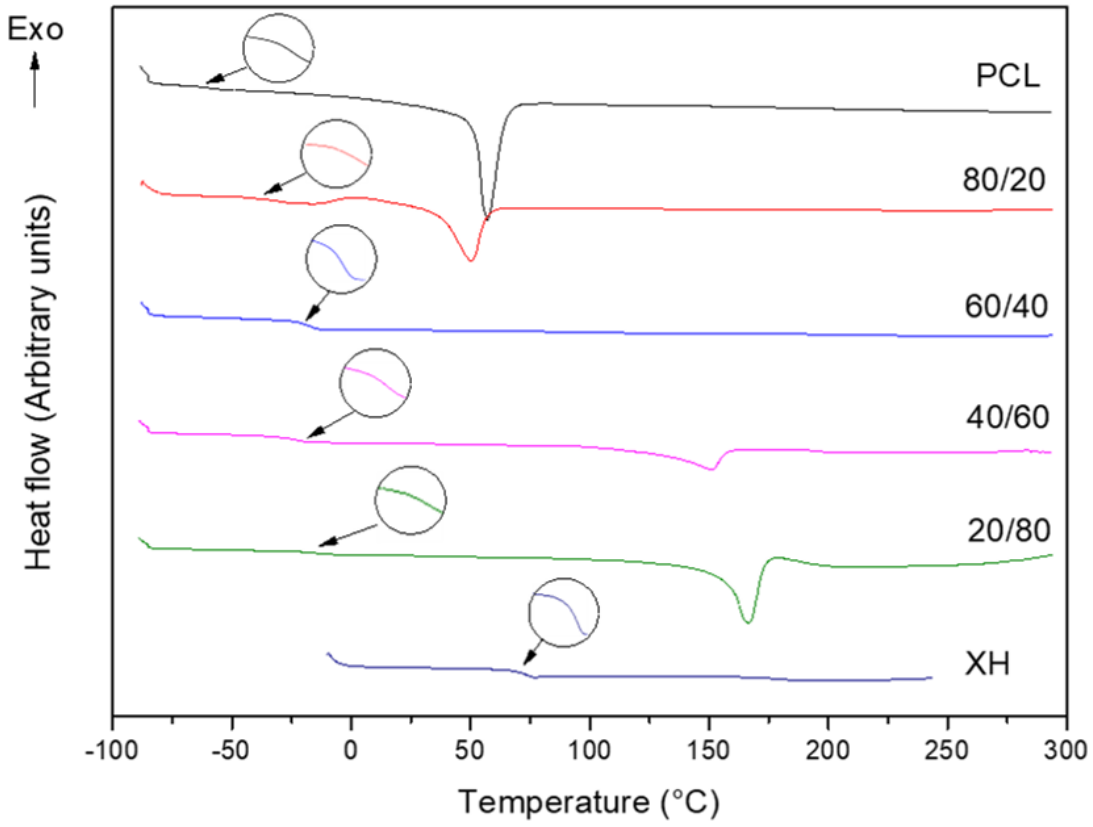

Figure 1. Second scan DSC traces for PCL, XH and PCL/XH blends.

Different methods, such as Gordon-Taylor (GT), Couchman-Karasz (CK) or Fox equations, have been employed to predict the glass transition temperature of amorphous binary systems. Particularly, the Gordon-Taylor equation was derived assuming ideal

solution behavior; and considering also equal densities, the widely used Fox equation (Eq. 1) can be derived [48]:

$$\frac{1}{T_{gb}} = \frac{w_1}{T_{g1}} + \frac{w_2}{T_{g2}} \quad (1)$$

where w_1 and w_2 are the weight fractions of components 1 and 2 respectively, T_{g1} and T_{g2} are the glass transition temperatures of the pure components, and T_{gb} is the glass transition temperature of the blend. As can be seen in Figure 2, in the 0-40 XH wt% range the experimental values are close to the values predicted by the Fox law, while at higher XH concentrations the experimental T_gs lie below the predicted values. This behavior can be rationalized considering that XH is completely dissolved in the PCL rich blends, while partial XH crystallization occurs in the XH rich blends (see also Fig.1) [46].

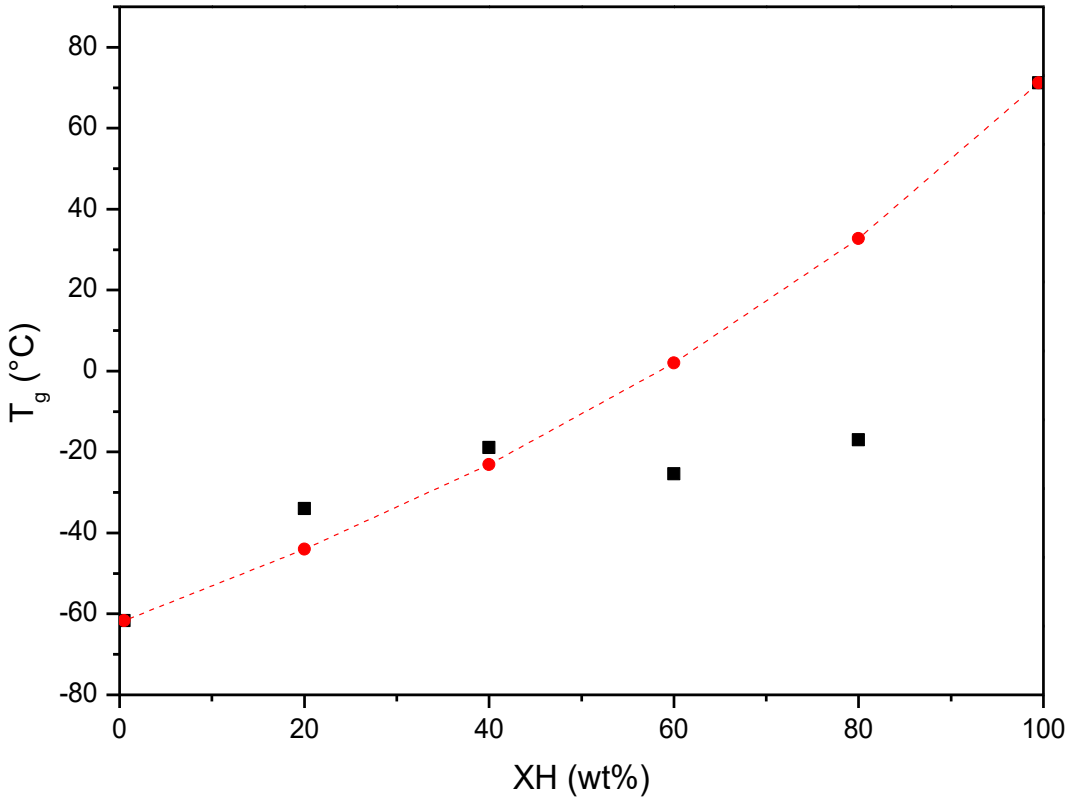

Figure 2. Glass transition temperature versus composition for the PCL/XH system: (■) experimental values (♦) Fox equation.

3.2. Melting Point Depression Analysis

Table 1 lists the melting properties of the pure components investigated in this work. As can be seen, PCL is a semicrystalline polymer melting at about 57°C, in good agreement with the values reported in the literature [45], [49]. However, the DSC scans performed on XH reveal an unusually large melting temperature dependence on heating rate, since its melting temperature increases by about 20ºC when the heating rate increases from 1ºC/min to 20ºC/min. A revision of the literature also reveals a broad range of melting temperatures reported for XH, ranging from 148ºC to 172ºC [50]–[53]. The dependence of melting temperature on heating rate is typical of compounds exhibiting "apparent melting", a new term proposed by Lee et al. [54] to distinguish the loss of crystalline structure caused by kinetic processes (e.g., thermal decomposition, dehydration, and chemical interactions/reactions) from that caused by thermodynamic melting. The apparent melting of sucrose (and other related compounds) was initially attributed to the kinetic process of thermal decomposition [54], but Magoń et al. [55] have recently shown it to be actually due to superheating. The melting of crystalline sucrose was found to be kinetically slow and under heating rates faster than equilibrium conditions the melting of crystals occurred at higher temperatures [55]. A similar behavior is observed in this work for XH. Even though degradation of XH to isoxanthohumol can occur upon melting [50], our samples did not show weight loss or decoloration during the DSC experiments, and similarly to sucrose, the observed dependence of melting temperature with heating rate can be attributed to the superheating of the XH crystals. The recommendation to obtain the equilibrium transition parameters for this type of compounds is to perform extrapolations to zero heating rate [55]. In any case, superheating is reduced with decreasing heating rate, hence only the measurements performed at sufficiently low heating rate (1ºC/min) will be used to analyze the melting point of XH in this section [56], [57].

Table 1. Melting properties of PCL and XH obtained from the first heating scans.

Compound (scan rate)	T_m (°C)	ΔH_m (J/g)
PCL	57.0	81
XH (20ºC/min)	173.2	121
XH (1ºC/min)	153.1	80

The melting point depression method, derived from the Flory-Huggins Theory, provides a thermodynamic description of the miscibility between two components. Essentially, a pure component melts when the entropic contribution ($T\Delta S_m$, arising from the increase in entropy upon melting) equals the enthalpic contribution (ΔH_m, arising from reduced intermolecular interactions in the liquid phase). However, in the presence of a second miscible component in liquid form, there is an additional entropic contribution arising for the combinatorial entropy, and an additional enthalpic contribution arising from intermolecular interactions with the second component. Both contributions shift the melting temperature of the pure component [58]. The Flory's relationship for the depression of the equilibrium melting point, ΔT_m, is (Eq. 2):

$$\frac{1}{T_m} - \frac{1}{T_m^0} = \frac{-R}{\Delta H_{2u}} \frac{V_{2u}}{V_{1u}} \left(\frac{\ln \phi_2}{m_2} + \left(\frac{1}{m_2} - \frac{1}{m_1} \right) \phi_1 + \chi_{12} \phi_1^2 \right) \quad (2)$$

where T_m^0 is the equilibrium melting point of the pure crystallizable component and T_m is the equilibrium melting point of its blends, the subscripts 1 and 2 refer to the amorphous and crystallizable components respectively. R is the universal gas constant, while ΔH_{2u} is the heat of fusion per mole of crystalline repeat units. V_u is the molar volume of the repeating unit, m is the degree of polymerization, ϕ is the volume fraction, and χ_{12} is the interaction parameter.

In order to analyze the melting point depression of XH (component 2) applying (Eq. 2), the molar volume of the lattice sites can be considered as the molar volume of XH ($V_2 = 285.8$ cm^3/mol, estimated from its crystalline density), and consequently $m_2 = 1$. To further simplify the equation, the same volume can be taken as the molar volume of the polymeric repeat unit ($V_2 = V_{1u}$). Since $m_1 = V_{pol}/V_{1u}$ is large, $1/m_1 \approx 0$. As a result, Eq. 2 reduces to:

$$\frac{1}{T_m} - \frac{1}{T_m^0} = \frac{-R}{\Delta H_2}(\ln \phi_2 + \phi_1 + \chi \phi_1^2) \quad (3)$$

where the first two terms in the right-hand side of Eq. (3) represent the mixing entropy contribution to ΔT_m, and the third term the mixing enthalpy contribution. Substituting typical numbers for a polymer-monomer system in Eq. 3, it is easy to show that the entropic term only accounts for a small depression (usually about 1–2º C) [44].

The average melting point of pure XH obtained at low heating rate (1°C/min) is $T_m^0 = 153.1$°C. The melting point decreases by about 5°C when 20 wt% PCL is added. Considering the average melting enthalpy of pure XH (ΔH_{XH} = 80 J/g), Eq. (4) has been used in Figure 3 to obtain the interaction parameter from the slope of the plot, χ = -1.3. This value confirms a thermodynamically miscible system, since negative values for the interaction parameter indicate an exothermic process, as expected when the interassociation interactions are stronger than the autoassociation interactions [58]. Additionally, it is possible to calculate the interaction energy density, B, at the melting temperature of XH according to Eq. (4):

$$\chi = \frac{B V_r}{RT} \quad (4)$$

where V_r is a reference volumen ($V_r = V_2 = 285.8$ cm^3/mol), yielding $B = -16$ J/cm^3.

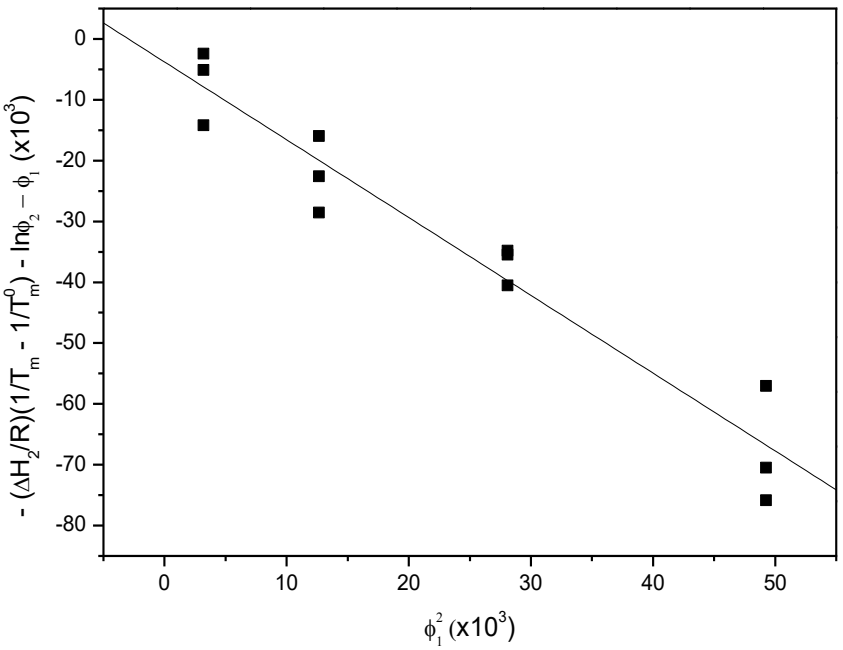

Figure 3. Analysis of the melting temperature of XH according to Eq. (4) for the PCL/XH system. The slope of the plot gives the interaction parameter χ = -1.3.

3.3. FTIR analysis of PCL/XH blends.

Hydrogen bonding interactions between the hydroxyl groups of XH and the carbonyl groups of PCL can be expected considering the chemical structures of the species investigated in this paper (see Sch. 1), hence, the occurrence of specific interactions has been investigated by infrared spectroscopy. Figure 4 shows the ester carbonyl stretching region of the pure components and their blends at room temperature (notice that the absorption region corresponding to the aromatic ketone present in XH occurs at lower wavenumbers and is not displayed in Fig. 4). The spectrum of pure PCL shows a peak at 1725 cm^{-1} attributable to crystalline PCL and a shoulder at 1735 cm^{-1} representing the amorphous phase [59]. As can be seen, blending with XH results in the occurrence of a new band located at about 1703 cm^{-1}, attributable to hydrogen bonded C=O groups in PCL[34]. The observed red shift (~32 cm^{-1}) is larger than those reported for blends of PCL with thymol [44] or chloramphenicol [60] (~25 cm^{-1}) indicating stronger hydrogen bonding interactions.

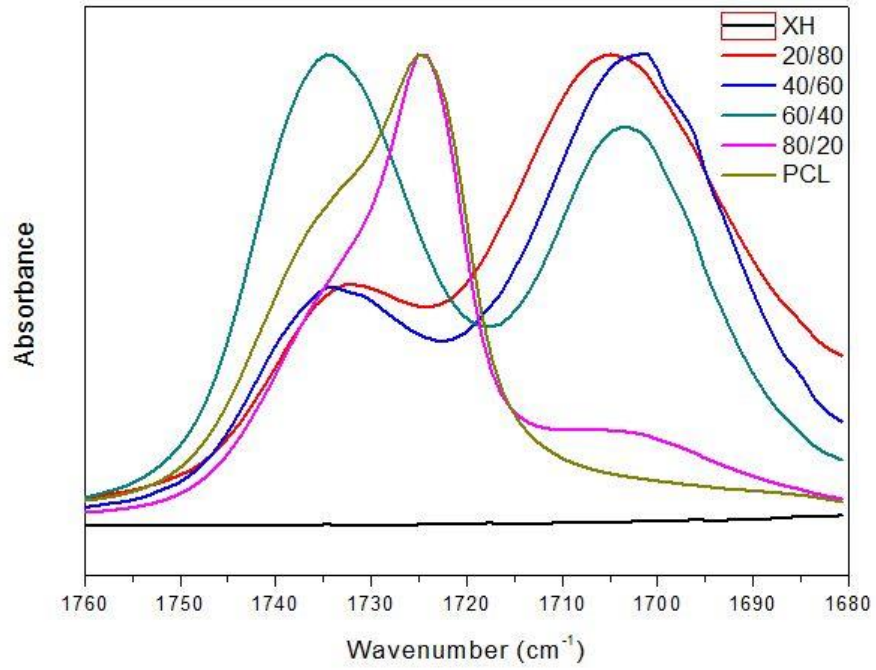

Figure 4. Carbonyl stretching region for pure PCL and XH and PCL/XH blends of different composition.

Figure 5 displays the hydroxyl stretching region of PCL and PCL/XH blends. The spectrum of pure XH shows a very broad band, attributable to the overlap of bands corresponding to different hydrogen bonding interactions. The typical location reported for pure completely dry XH, about 3300 cm^{-1} [61] indicates the occurrence of cooperative O-H···O-H interactions [60], though the actual location observed can be affected by residual water or other compounds that may cocrystallize with the pure compound [62], [63]. As can be seen, the addition of PCL to XH shifts the band to higher wavenumbers, up to about 3350 cm^{-1} as the PCL content in the blend increases. Shifting to higher wavenumbers is usually attributed to the replacement of the cooperatively strengthened hydroxyl-hydroxyl interactions by the weaker hydroxyl-carbonyl interactions absorbing at higher wavenumbers [60], [64].

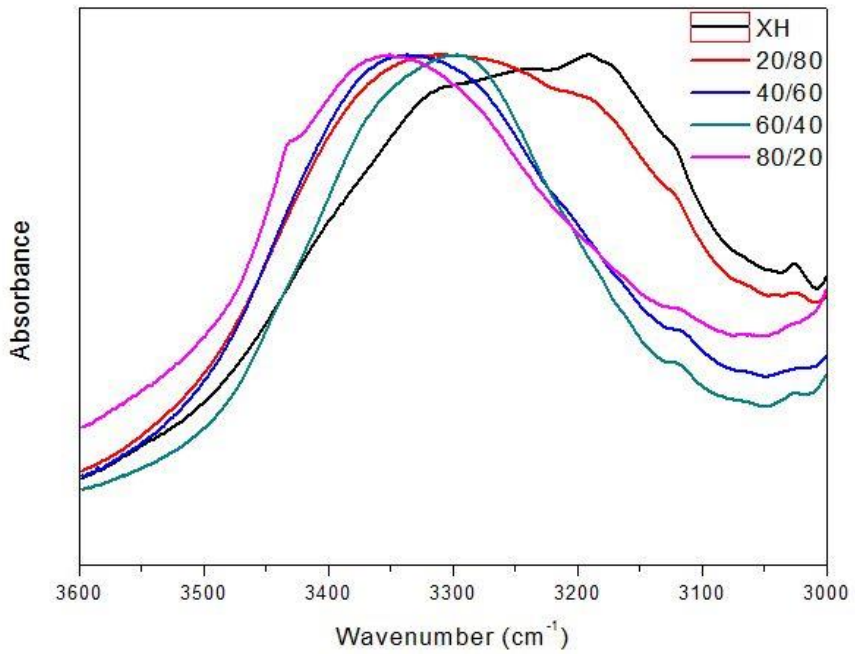

Figure 5. Hydroxyl stretching region for pure XH and PCL/XH blends of different composition.

3.4. Crystallization Behavior Based on the X-ray Diffraction Analysis

The XRD patterns of the pure components are shown in Figure 6. XH exhibits characteristic peaks at 2θ = 5.8° and 7.7° with several peaks between 11° and 28°, while the characteristic peaks of PCL occur at 2θ = 21.7° and 24°. As can be seen, the intensity of the crystalline peaks of XH decreases with the addition of PCL. The same behavior is observed for the PCL peaks upon increasing the XH content. For the PCL/XH 60/40 composition, the material is an homogeneous, single phase blend. If the XH content is increased to 50 wt%, the XRD diffraction pattern shows a weak, broad peak centered at about 2θ = 6.6°, shifted form the locations corresponding to the pure XH crystals. This suggests that at this composition XH is still unable to form fully developed crystals, and the peak arises from small ordered regions intimately connected to the surrounding amorphous matrix [24]. Further increase of the XH content to 60 wt% results in the occurrence of a fully developed second phase consisting of pure XH crystals, though the mass fraction corresponding to this second phase is still small according to the intensity of the crystalline peaks.

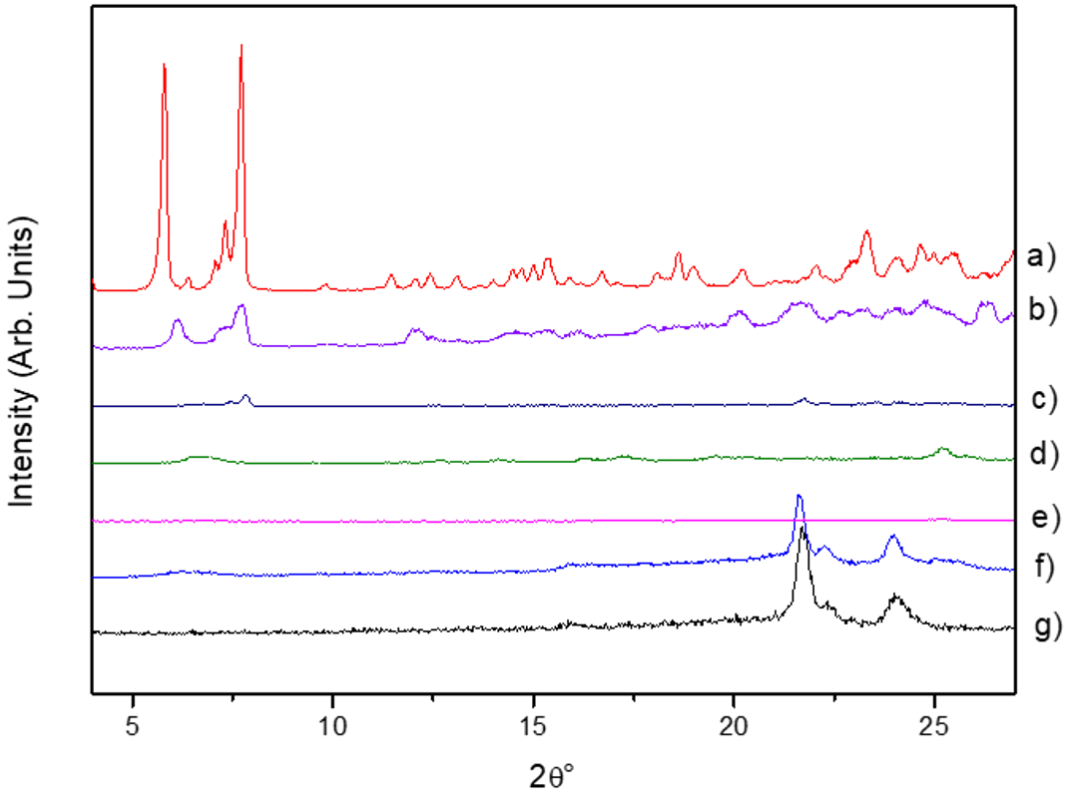

Figure 6. XRD patterns of: a) pure XH; b) PCL/XH 30/70; c) PCL/XH 40/60; d) PCL/XH 50/50; e) PCL/XH 60/40; f) PCL/XH 70/30 and g) pure PCL.

3.4. AFM Analysis

Figure 7 shows topographic images of thin films (400 nm) of pure PCL and PCL/XH blends of different compsition obtained by Atomic Force Microscopy. As can be seen, pure PCL shows the characteristic spherulitic morphology of semicrystalline polymers. Upon addition of 20 wt% XH, spherulitic boundaries become less defined, and the crystalline phase shows a looser, less compact morphology, indicating that crystallization of PCL in the presence of XH creates a XH enriched amorphous phase that is displaced by the growing crystallites to the interlamellar region and to the spherulitic grain boundaries [65]. On the other hand, the PCL/XH 40/60 system shows discrete XH crystals dispersed in a smooth and homogeneous film. In case of the intermediate PCL/XH 60/40 composition, the topographic images obtained lack any crystalline morphology in agreement with the XRD analysis, but show a rough surface that suggests the occurrenve of compositional heterogeneities attributable to a metaestable composition

[66]. The analysis of the long term stability of this system is, however, beyond the scope of this paper.

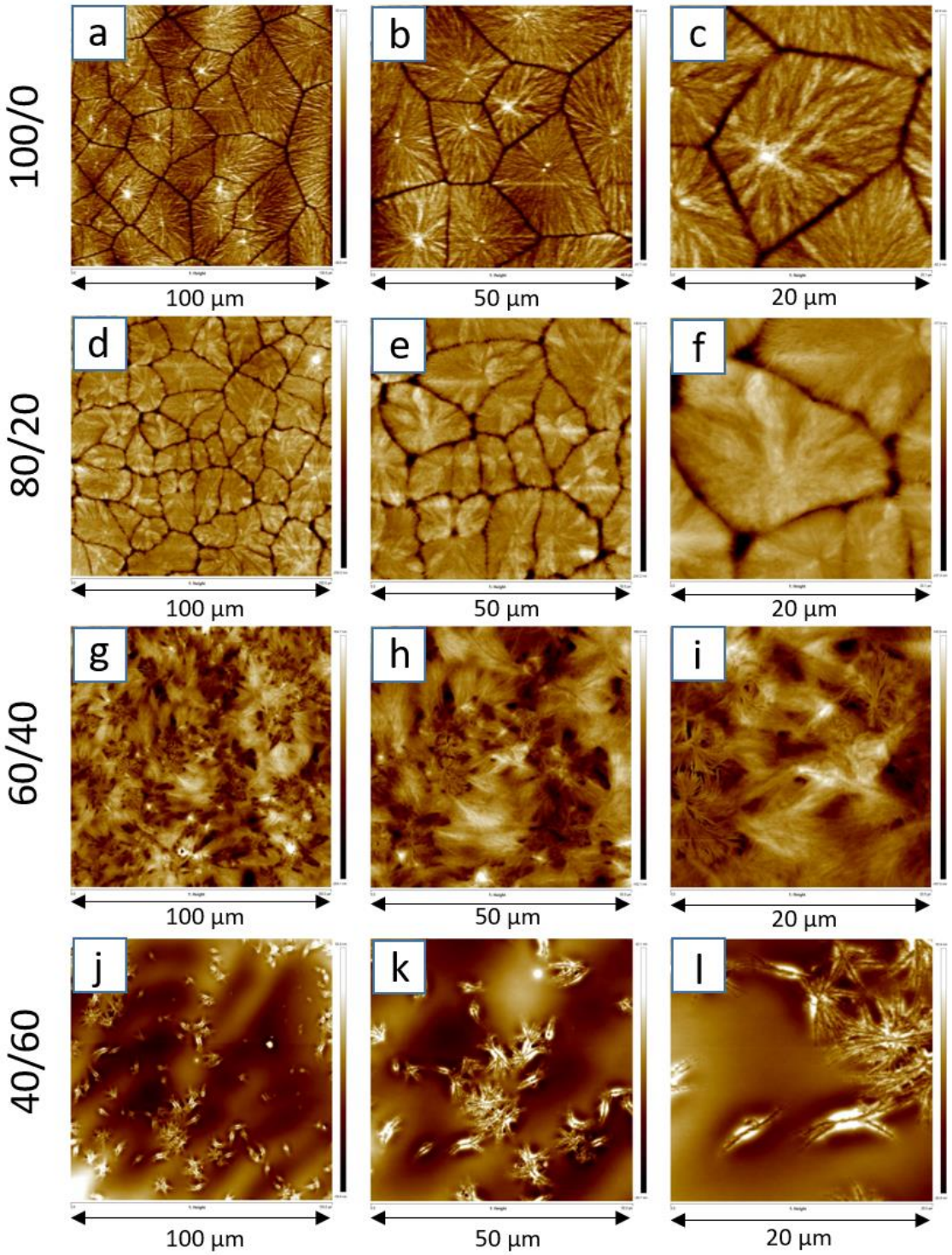

Figure 7. AFM topographic images for pure PCL and PCL/XH blends of different compsition.

3.6. Tensile Behavior

The tensile behavior of PCLs is strongly dependent on molecular weight [67]. PCL oligomers (M_w below several thousands) are brittle and waxy, but both ductility and tensile modulus increase with increasing molecular weight [68]. Low molecular weight PCLs (M_w from 10^4 to a few tens of thousands) are soft and show increased ductility, while high molecular weight PCL achieves mechanical properties comparable to linear polyethylenes, reaching Young's modulus E = 700 MPa and elongation at break in the 700-1000% range [67], [69]. Figure 8 shows the tensile curves obtained for the high molecular weight PCL sample investigated in this work and its blends containing up to 60 wt% XH. As can be seen, the tensile curves of the blends lie below that of pure PCL, indicating that the addition of XH reduces the resistive properties of the blends. This behavior should be attributed to the suppression of the crystallinity of PCL occurring upon the addition of XH rather than to a plasticizing effect, since the addition of XH actually increases the glass transition of the blends. Interestingly, the blends retain high ductilities within the composition range in which XH is dispersed in amorphous form. For example, adding 50 wt% XH to PCL reduces the strain at break from $\varepsilon_b = 595 \pm 25$ % to $\varepsilon_b = 374 \pm 7$ %, hence the films retain nearly 2/3 of the ductility in spite of containing half the polymer. However, a strong reduction of ductility is observed when the XH content increases further to 60 wt% ($\varepsilon_b = 135 \pm 21$ %). The strong reduction of ductility observed upon increasing the XH content from 50 wt% to 60 wt% cannot be explained only in terms of the lower polymer content of the latter. In this case, the presence of a disruptive second crystalline phase in the sample containing 60 wt% XH must be considered as an additional detrimental effect.

.

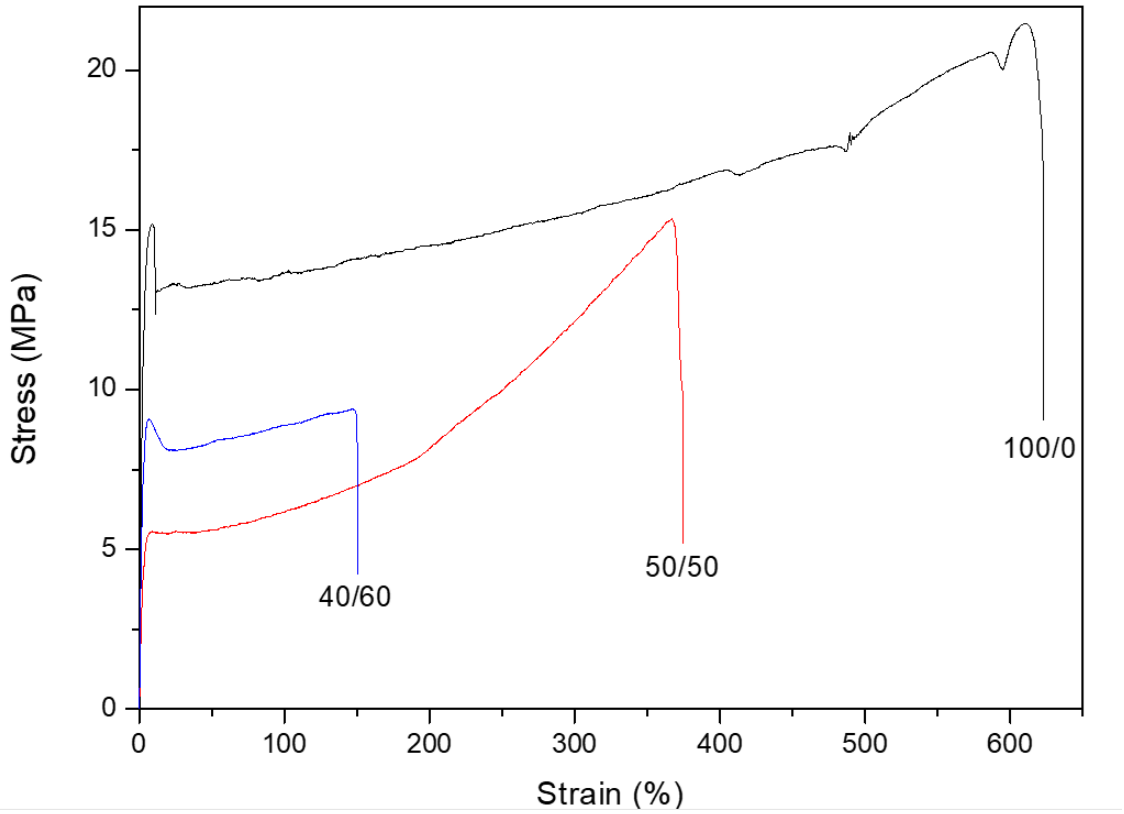

Figure 8. Tensile tests for the PCL/XH blends.

Figure 9 shows the Young's modulus and the yield stress for pure PCL and its blends with XH of different composition. The Young's modulus for the pure PCL used in this work is 686 ± 2 MPa (see Fig. 9a), in good agreement with values reported in the literature [60]. As can be seen, the addition of XH to PCL halves the stiffness of the films. In addition, the yield strength of pure PCL (15.4 ± 0.7 MPa, see Fig. 9b) is also halved upon the addition of XH. A dependence on composition cannot be established for these parameters from our results. In any case, the analysis of the mechanical properties shows that soft, flexible PCL/XH blends can be developed, particularly by considering also the possibility of tuning the molecular weight of PCL to achieve the desired mechanical properties.

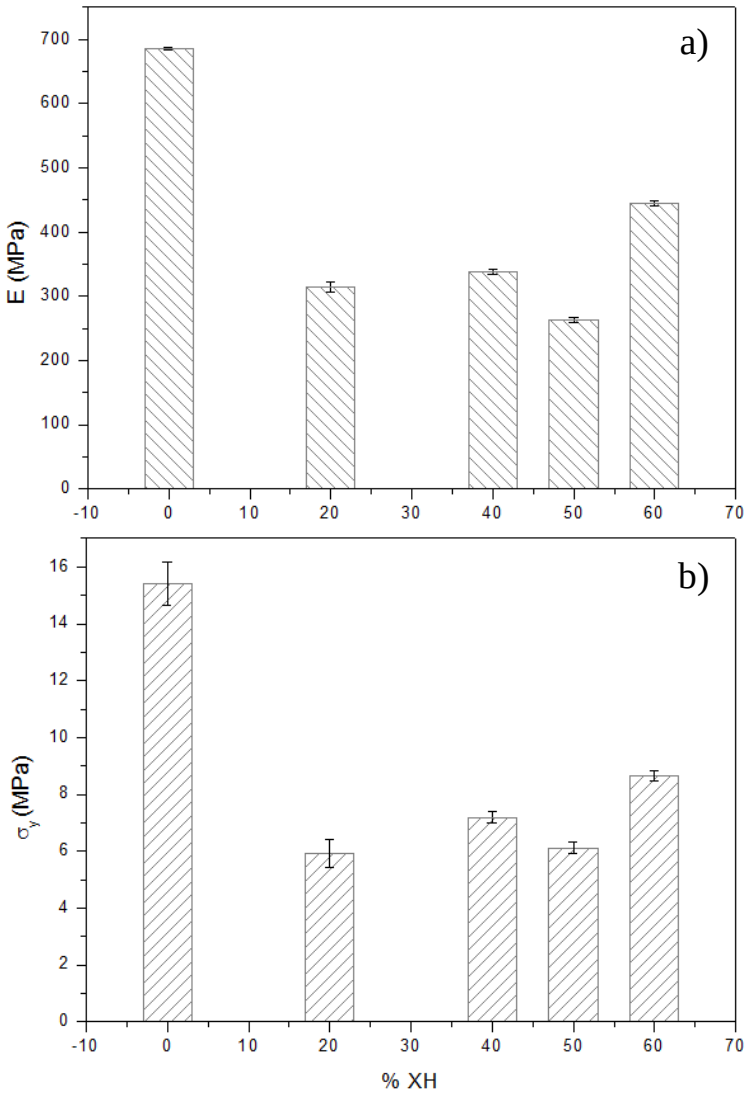

Figure 9. a) Young's modulus and b) yield stress values for PCL and PCL/XH blends.

Table 2. Statistical analysis results for the mechanical properties.

XH wt%	YOUNG'S MODULUS		YIELD STRENGTH	
	Average modulus (MPa)	Standard deviation	Average Yield strength (MPa)	Standard deviation
0	685.8	±2.0	15.4	±0.7
20	314.9	±8.3	5.9	±0.5
40	338.5	±4.6	7.2	±0.2
50	263.3	±3.1	6.1	±0.2
60	444.7	±3.9	8.6	±0.2

3.7. Drug Release Behavior

As indicated in the introduction, XH is virtually insoluble in water due to its non-polar, highly hydrophobic nature. The solubility reported in aqueous media is 1.3 mg/L (about 1.3 ppm) at 23º C [70]. Such a low value limits its bioavalavility and makes difficult handling XH to perform both in vivo and in vitro pharmacological studies [62]. Hence, solubility and drug release studies have been usually carried out in 50:50 (v/v) ethanol–water solution, where the solubility of XH increases to 7.6 mg/L [62].

In an attempt to stick as close as possible to the physiological conditions, release experiments have been carried out in 0.1 M PBS (pH 7.4) medium. To avoid the precipitation of XH (usually occurring when the solutions reach the unstable region of the phase diagram), the total XH concentration has been limited by removing the whole solution before each addition of fresh PBS medium. Figure 10 shows the in vitro drug release profiles for the PCL/XH blends containing 2, 5 and 10 wt% XH. As can be seen, in the experimental conditions chosen for this analysis, all the samples show quasi-linear release profiles, and the whole drug was released in short time lapses, of about 1 hour, 3 hours and 4.5 hours respectively. The XH released in each step reached 50 μg (in 4 ml of PBS solution), hence, XH concentrations of about 12 mg/L were achieved without precipitation in the release experiments. Both the larger XH concentrations and the short release times indicate that releasing from PCL/XH ASDs should increase the bioavailability of the drug.

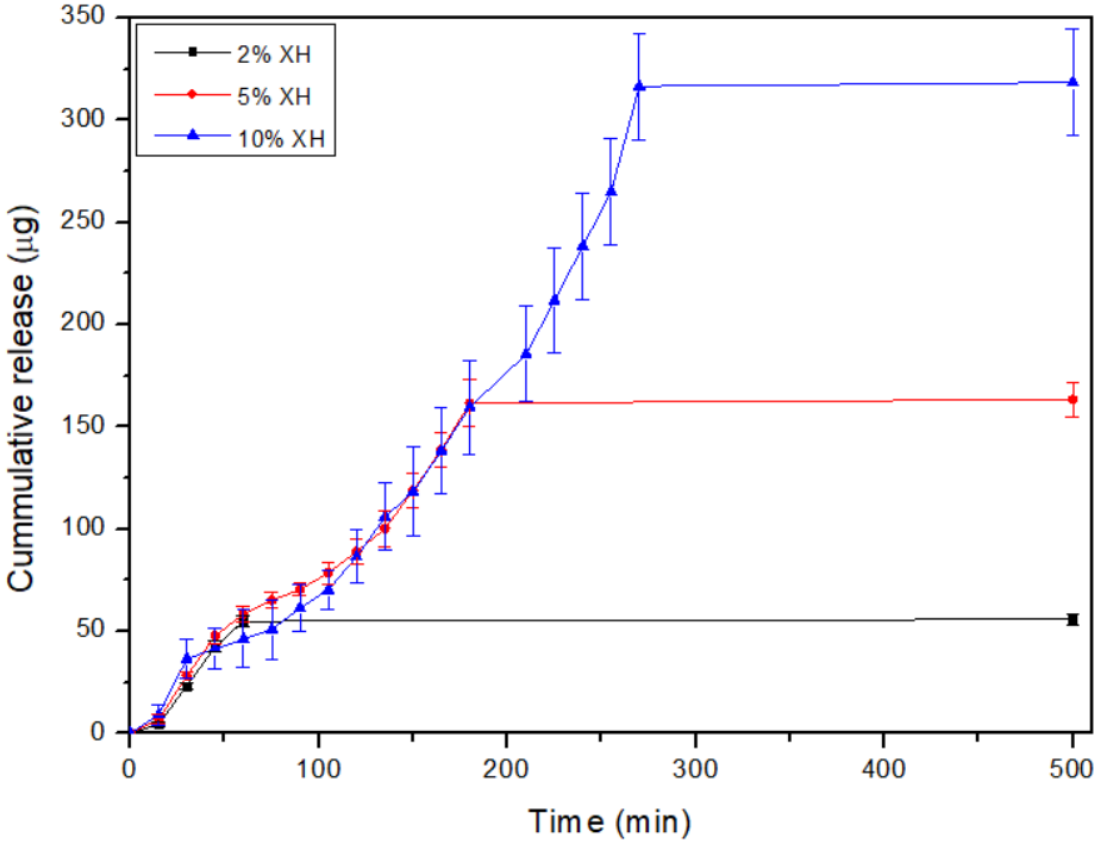

Figure 10. Drug release profiles of PCL/XH films containing 2, 5 and 10 wt% XH immersed into 0.1 M PBS buffer at 37º C.

4. Conclusions

Miscibility is observed in the PCL/XH system according to the intermediate glass transition temperature criterion. The analysis of the melting point depression of the XH crystals results in a negative interaction parameter, χ = -1.3, indicating favorable interactions between the polymer and the bioactive molecule. Crystallization is suppressed for both PCL or XH in the presence of the second component. In fact, the PCL/XH 60/40 blend is completely amorphous according to both the DSC and X-Ray diffraction pattern analyses. PCL can be loaded with XH contents up to 50 wt% to obtain amorphous solid dispersions (ASDs) of the bioactive molecule.

The analysis by FTIR spectroscopy for the PCL/XH blends shows new bands in the C=O stretching region attributable to C=O···H-O interactions between the carbonyl groups of PCL and the hydroxyl groups of XH. In addition, the hydroxyl stretching band of XH shifts to higher wavenumbers in the presence of PCL indicating the replacement

of the cooperative H-O···H-O autoassociation interactions by C=O···H-O interassociation interactions.

The analysis of the spherulitic morphology of the blends by AFM shows that the addition of XH to PCL results in less defined spherulites, showing a looser, less compact morphology, characteristic of miscible systems. Tensile tests indicate that the resistant properties of PCL are reduced upon the addition of XH, but the materials maintain high ductilities even in the presence of XH contents up to 50 wt%. The PCL/XH system shows interesting properties for the development of biomedical devices based on soft materials.

Conflicts of interest

There are no conflicts of interest to declare.

Acknowledgements

Financial support from the Spanish Ministry of Science and Innovation MICINN (PID2019-106236GB-I00) and the Basque Government Department of Education, Culture and Language Policy (IT-927-16) is gratefully acknowledged. The authors thank for technical and human support provided by SGIker of UPV/EHU and European funding (ERDF and ESF).

References

[1] R. M. Donlan, “Biofilms: Microbial life on surfaces,” *Emerg. Infect. Dis.*, vol. 8, no. 9, pp. 881–890, 2002, doi: 10.3201/eid0809.020063.

[2] R. M. Donlan, “Biofilms and device-associated infections,” *Emerg. Infect. Dis.*, vol. 7, no. 2, pp. 277–281, 2001, doi: 10.3201/eid0702.010226.

[3] S. Aiola, G. Amico, P. Battaglia, and E. Battistelli, “The Large-Scale Polarization Explorer (LSPE),” *Clin. Microbiol. Rev.*, vol. 15, no. 2, pp. 167–193, 2002, doi: 10.1128/CMR.15.2.167.

[4] M. Palomar, J. Vaque, F. Álvarez Lerma, V. Pastor, P. Olaechea, and J. Fernández-Crehuet, “Indicadores de infección nosocomial,” *Med. Clin. (Barc).*, vol. 131, pp. 48–55, 2008, doi: https://doi.org/10.1016/S0025-7753(08)76461-3.

[5] G. Ducel, J. Fabry, and L. Nicole, “Prevention of hospital-acquired infections: A practical guide,” 2002. [Online]. Available: https://www.who.int/csr/resources/publications/WHO_CDS_CSR_EPH_2002_12/en/.

[6] J. W. Costerton, P. S. Stewart, and E. P. Greenberg, “Bacterial biofilms: A common cause of persistent infections,” *Science (80-.).*, vol. 284, no. 5418, pp. 1318–1322, 1999, doi: 10.1126/science.284.5418.1318.

[7] M. R. Parsek and P. K. Singh, “Bacterial Biofilms: An Emerging Link to Disease Pathogenesis,” *Annu. Rev. Microbiol.*, vol. 57, no. 1, pp. 677–701, 2003, doi: 10.1146/annurev.micro.57.030502.090720.

[8] C. A. Fux, J. W. Costerton, P. S. Stewart, and P. Stoodley, “Survival strategies of infectious biofilms,” *Trends Microbiol.*, vol. 13, no. 1, pp. 34–40, 2005, doi: 10.1016/j.tim.2004.11.010.

[9] C. M. Kirschner and A. B. Brennan, “Bio-Inspired Antifouling Strategies,” *Annu. Rev. Mater. Res.*, vol. 42, no. 1, pp. 211–229, 2012, doi: 10.1146/annurev-matsci-070511-155012.

[10] N. Fusetani, “Antifouling marine natural products,” *Nat. Prod. Rep.*, vol. 28, no. 2, pp. 400–410, 2011, doi: 10.1039/c0np00034e.

[11] K. Bazaka, M. V. Jacob, W. Chrzanowski, and K. Ostrikov, “Anti-bacterial surfaces: Natural agents, mechanisms of action, and plasma surface modification,” *RSC Adv.*, vol. 5, no. 60, pp. 48739–48759, 2015, doi:

10.1039/c4ra17244b.

[12] P. Y. Qian, Y. Xu, and N. Fusetani, “Natural products as antifouling compounds: recent progress and future perspectives.,” *Biofouling*, vol. 26, no. 2, pp. 223–234, 2010, doi: 10.1080/08927010903470815.

[13] J. R. Almeida and V. Vasconcelos, “Natural antifouling compounds: Effectiveness in preventing invertebrate settlement and adhesion,” *Biotechnol. Adv.*, vol. 33, no. 3–4, pp. 343–357, 2015, doi: 10.1016/j.biotechadv.2015.01.013.

[14] H. X. Xu and S. F. Lee, “Activity of plant flavonoids against antibiotic-resistant bacteria,” *Phyther. Res.*, vol. 15, no. 1, pp. 39–43, 2001, doi: 10.1002/1099-1573(200102)15:1<39::AID-PTR684>3.0.CO;2-R.

[15] T. P. T. Cushnie and A. J. Lamb, “Antimicrobial activity of flavonoids,” *Int. J. Antimicrob. Agents*, vol. 26, no. 5, pp. 343–356, 2005, doi: 10.1016/j.ijantimicag.2005.09.002.

[16] X. Zhou *et al.*, “Flavone and isoflavone derivatives of terrestrial plants as larval settlement inhibitors of the barnacle Balanus amphitrite,” *Biofouling*, vol. 25, no. 1, pp. 69–76, 2009, doi: 10.1080/08927010802455941.

[17] S. Kumar and A. K. Pandey, “Chemistry and biological activities of flavonoids: An overview,” *Sci. World J.*, vol. 2013, no. 7, pp. 637–670, 2013, doi: 10.1155/2013/162750.

[18] A. Córdoba *et al.*, “Flavonoid-modified surfaces: Multifunctional bioactive biomaterials with osteopromotive, anti-inflammatory, and anti-fibrotic potential,” *Adv. Healthc. Mater.*, vol. 4, no. 4, pp. 540–549, 2015, doi: 10.1002/adhm.201400587.

[19] M. Liu *et al.*, “Pharmacological profile of xanthohumol, a prenylated flavonoid from hops (Humulus lupulus),” *Molecules*, vol. 20, no. 1, pp. 754–779, 2015, doi: 10.3390/molecules20010754.

[20] E. Sangiovanni *et al.*, “A bio-guided assessment of the anti-inflammatory activity of hop extracts (Humulus lupulus L. cv. Cascade) in human gastric epithelial cells,” *J. Funct. Foods*, vol. 57, no. April, pp. 95–102, 2019, doi: 10.1016/j.jff.2019.03.041.

[21] J. L. Bolton *et al.*, “The Multiple Biological Targets of Hops and Bioactive Compounds,” *Chem. Res. Toxicol.*, vol. 32, no. 2, pp. 222–233, 2019, doi: 10.1021/acs.chemrestox.8b00345.

[22] M. Ambrož, K. Lněničková, P. Matoušková, L. Skálová, and I. Boušová, "Antiproliferative effects of hop-derived prenylflavonoids and their influence on the efficacy of oxaliplatine, 5-fluorouracil and irinotecan in human colorectalC cells," *Nutrients*, vol. 11, no. 4, 2019, doi: 10.3390/nu11040879.

[23] J. Sastre-Serra, Y. Ahmiane, P. Roca, J. Oliver, and D. G. Pons, "Xanthohumol, a hop-derived prenylflavonoid present in beer, impairs mitochondrial functionality of SW620 colon cancer cells," *Int. J. Food Sci. Nutr.*, vol. 70, no. 4, pp. 396–404, 2019, doi: 10.1080/09637486.2018.1540558.

[24] J. M. Seliger, H. J. Martin, E. Maser, and J. Hintzpeter, "Potent inhibition of human carbonyl reductase 1 (CBR1) by the prenylated chalconoid xanthohumol and its related prenylflavonoids isoxanthohumol and 8-prenylnaringenin," *Chem. Biol. Interact.*, vol. 305, no. January, pp. 156–162, 2019, doi: 10.1016/j.cbi.2019.02.031.

[25] A. Sławińska-Brych *et al.*, "Xanthohumol exhibits anti-myeloma activity in vitro through inhibition of cell proliferation, induction of apoptosis via the ERK and JNK-dependent mechanism, and suppression of sIL-6R and VEGF production," *Biochim. Biophys. Acta - Gen. Subj.*, vol. 1863, no. 11, 2019, doi: 10.1016/j.bbagen.2019.08.001.

[26] N. Yamaguchi, K. Satoh-Yamaguchi, and M. Ono, "In vitro evaluation of antibacterial, anticollagenase, and antioxidant activities of hop components (Humulus lupulus) addressing acne vulgaris," *Phytomedicine*, vol. 16, no. 4, pp. 369–376, 2009, doi: 10.1016/j.phymed.2008.12.021.

[27] S. Bhattacharya, S. Virani, M. Zavro, and G. J. Haas, "Inhibition of Streptococcus mutans and other oral Streptococci by hop (Humulus lupulus L.) constituents," *Econ. Bot.*, vol. 57, no. 1, pp. 118–125, 2003, doi: 10.1663/0013-0001(2003)057[0118:IOSMAO]2.0.CO;2.

[28] C. Gerhäuser, "Broad spectrum antiinfective potential of xanthohumol from hop (Humulus lupulus L.) in comparison with activities of other hop constituents and xanthohumol metabolites," *Mol. Nutr. Food Res.*, vol. 49, no. 9, pp. 827–831, Sep. 2005, doi: 10.1002/mnfr.200500091.

[29] N. Zhang, Z. Liu, Q. Han, J. Chen, and Y. Lv, "Xanthohumol enhances antiviral effect of interferon α-2b against bovine viral diarrhea virus, a surrogate of hepatitis C virus," *Phytomedicine*, vol. 17, no. 5, pp. 310–316, 2010, doi: https://doi.org/10.1016/j.phymed.2009.08.005.

[30] Q. Wang, Z.-H. Ding, J.-K. Liu, and Y.-T. Zheng, “Xanthohumol, a novel anti-HIV-1 agent purified from Hops Humulus lupulus,” *Antiviral Res.*, vol. 64, no. 3, pp. 189–194, 2004, doi: https://doi.org/10.1016/j.antiviral.2004.08.005.

[31] C. R. Langezaal, A. Chandra, and J. J. C. Scheffer, “Antimicrobial screening of essential oils and extracts of someHumulus lupulus L. cultivars,” *Pharm. Weekbl.*, vol. 14, no. 6, pp. 353–356, 1992, doi: 10.1007/BF01970171.

[32] Oyvind M. Andersen and K. R. Markham, *Flavonoids: Chemistry, Biochemistry and Applications - 1st Edition - O.* .

[33] N. Sus *et al.*, “Validation of a rapid and sensitive reversed-phase liquid chromatographic method for the quantification of prenylated chalcones and flavanones in plasma and urine,” *NFS J.*, vol. 10, pp. 1–9, Mar. 2018, doi: 10.1016/j.nfs.2017.11.001.

[34] N. López-Rodríguez, A. López-Arraiza, E. Meaurio, and J. R. Sarasua, “Crystallization, morphology, and mechanical behavior of polylactide/poly(ε-caprolactone) blends,” *Polym. Eng. Sci.*, vol. 46, no. 9, pp. 1299–1308, 2006, doi: 10.1002/pen.20609.

[35] L. Di and E. H. Kerns, “Solubility,” in *Drug-Like Properties*, Elsevier, 2016, pp. 61–93.

[36] P.-Y. Qian, Y. Xu, and N. Fusetani, “Natural products as antifouling compounds: recent progress and future perspectives,” *Biofouling*, vol. 26, no. 2, pp. 223–234, 2009, doi: 10.1080/08927010903470815.

[37] B. T. Surikutchi, S. P. Patil, G. Shete, S. Patel, and A. K. Bansal, “Drug-excipient behavior in polymeric amorphous solid dispersions,” *J. Excipients Food Chem. Vol 4 No 3*, Sep. 2013, [Online]. Available: https://ojs.abo.fi/ojs/index.php/jefc/article/view/214.

[38] M. M. Knopp, N. E. Olesen, Y. Huang, R. Holm, and T. Rades, “Statistical Analysis of a Method to Predict Drug-Polymer Miscibility,” *J. Pharm. Sci.*, vol. 105, no. 1, pp. 362–367, Jan. 2016, doi: 10.1002/jps.24704.

[39] M. M. Knopp *et al.*, “Comparative Study of Different Methods for the Prediction of Drug–Polymer Solubility,” *Mol. Pharm.*, vol. 12, no. 9, pp. 3408–3419, 2015, doi: 10.1021/acs.molpharmaceut.5b00423.

[40] J. Tao, Y. Sun, G. G. Z. Zhang, and L. Yu, “Solubility of small-molecule crystals in polymers: D-Mannitol in PVP, indomethacin in PVP/VA, and nifedipine in PVP/VA,” *Pharm. Res.*, vol. 26, no. 4, pp. 855–864, Apr. 2009, doi:

10.1007/s11095-008-9784-z.

[41] P. J. Marsac, T. Li, and L. S. Taylor, “Estimation of Drug–Polymer Miscibility and Solubility in Amorphous Solid Dispersions Using Experimentally Determined Interaction Parameters,” *Pharm. Res.*, vol. 26, no. 1, pp. 139–151, 2008, doi: 10.1007/s11095-008-9721-1.

[42] K. DeBoyace and P. L. D. Wildfong, “The Application of Modeling and Prediction to the Formation and Stability of Amorphous Solid Dispersions,” *Journal of Pharmaceutical Sciences*, vol. 107, no. 1. Elsevier B.V., pp. 57–74, Jan. 01, 2018, doi: 10.1016/j.xphs.2017.03.029.

[43] T. Vasconcelos, B. Sarmento, and P. Costa, “Solid dispersions as strategy to improve oral bioavailability of poor water soluble drugs,” *Drug Discov. Today*, vol. 12, no. 23–24, pp. 1068–1075, 2007, doi: 10.1016/j.drudis.2007.09.005.

[44] E. Sanchez-Rexach, I. Martínez de Arenaza, J. R. Sarasua, and E. Meaurio, “Antimicrobial poly(ε-caprolactone)/thymol blends: Phase behavior, interactions and drug release kinetics,” *Eur. Polym. J.*, vol. 83, pp. 288–299, Oct. 2016, doi: 10.1016/j.eurpolymj.2016.08.029.

[45] E. Sanchez-Rexach *et al.*, “Miscibility, interactions and antimicrobial activity of poly(ε-caprolactone)/chloramphenicol blends,” *Eur. Polym. J.*, vol. 102, pp. 30–37, 2018, doi: 10.1016/j.eurpolymj.2018.03.011.

[46] R. Pezzoli, J. G. Lyons, N. Gately, and C. L. Higginbotham, “Investigation of miscibility estimation methods between indomethacin and poly(vinylpyrrolidone-co-vinyl acetate),” *Int. J. Pharm.*, vol. 549, no. 1–2, pp. 50–57, 2018, doi: 10.1016/j.ijpharm.2018.07.039.

[47] N. Hernandez-Montero, J. M. Ugartemendia, H. Amestoy, and J. R. Sarasua, “Complex phase behavior and state of miscibility in Poly(ethylene glycol)/Poly(l-lactide-co-ε-caprolactone) Blends,” *J. Polym. Sci. Part B Polym. Phys.*, vol. 52, no. 2, pp. 111–121, Jan. 2014, doi: 10.1002/polb.23394.

[48] J. A. Baird and L. S. Taylor, “Evaluation of amorphous solid dispersion properties using thermal analysis techniques,” *Adv. Drug Deliv. Rev.*, vol. 64, no. 5, pp. 396–421, 2012, doi: 10.1016/j.addr.2011.07.009.

[49] E. Meaurio, N. Hernandez-Montero, E. Zuza, and J. R. Sarasua, “Miscible Blends Based on Biodegradable Polymers,” in *Characterization of Polymer Blends: Miscibility, Morphology and Interfaces*, vol. 9783527331, Wiley Blackwell, 2015, pp. 7–92.

[50] R. S. Khupse and P. W. Erhardt, “Total synthesis of xanthohumol,” *J. Nat. Prod.*, vol. 70, no. 9, pp. 1507–1509, Sep. 2007, doi: 10.1021/np070158y.

[51] R. Hänsel and J. Schulz, “Desmethylxanthohumol: Isolierung aus Hopfen und Cyclisierung zu Flavanonen,” *Arch. Pharm. (Weinheim).*, vol. 321, no. 1, pp. 37–40, Jan. 1988, doi: 10.1002/ardp.19883210112.

[52] S. Song-San, S. Watanabe, and T. Saito, “Chalcones from Humulus lupulus,” *Phytochemistry*, vol. 28, no. 6, pp. 1776–1777, Jan. 1989, doi: 10.1016/S0031-9422(00)97849-X.

[53] F. Govaert, M. Verzele, M. Anteunis, F. Fontyn, and J. Stockx, “Xanthohumol,” *Experientia*, vol. 13, no. 3, pp. 105–106, 1957, doi: 10.1007/BF02157558.

[54] J. W. Lee, L. C. Thomas, and S. J. Schmidt, “Can the thermodynamic melting temperature of sucrose, glucose, and fructose be measured using rapid-scanning differential scanning calorimetry (DSC)?,” *J. Agric. Food Chem.*, vol. 59, no. 7, pp. 3306–3310, Apr. 2011, doi: 10.1021/jf104852u.

[55] A. Magoń *et al.*, “Heat capacity and transition behavior of sucrose by standard, fast scanning and temperature-modulated calorimetry,” *Thermochim. Acta*, vol. 589, pp. 183–196, Aug. 2014, doi: 10.1016/j.tca.2014.05.029.

[56] P. J. Marsac, T. Li, and L. S. Taylor, “Estimation of drug-polymer miscibility and solubility in amorphous solid dispersions using experimentally determined interaction parameters,” *Pharm. Res.*, vol. 26, no. 1, pp. 139–151, Jan. 2009, doi: 10.1007/s11095-008-9721-1.

[57] M. M. Knopp *et al.*, “Comparative Study of Different Methods for the Prediction of Drug-Polymer Solubility,” *Mol. Pharm.*, vol. 12, no. 9, pp. 3408–3419, Sep. 2015, doi: 10.1021/acs.molpharmaceut.5b00423.

[58] M. A. Altamimi and S. H. Neau, “A study to identify the contribution of Soluplus® component homopolymers to the solubilization of nifedipine and sulfamethoxazole using the melting point depression method,” *Powder Technol.*, vol. 338, pp. 576–585, 2018, doi: 10.1016/j.powtec.2018.07.027.

[59] E. G. Lezcano, C. Salom Coll, and M. G. Prolongo, “Melting behaviour and miscibility of poly(ϵ-caprolactone) + poly(4-hydroxystyrene) blends,” *Polymer (Guildf).*, vol. 37, no. 16, pp. 3603–3609, 1996, doi: https://doi.org/10.1016/0032-3861(96)00170-X.

[60] E. Meaurio, E. Sanchez-Rexach, A. Butron, and J.-R. Sarasua, “The conformation of chloramphenicol in the ordered and disordered phases,”

Spectrochim. Acta - Part A Mol. Biomol. Spectrosc., vol. 211, 2019, doi: 10.1016/j.saa.2018.12.021.

[61] M. Arczewska *et al.*, "The molecular organization of prenylated flavonoid xanthohumol in DPPC multibilayers: X-ray diffraction and FTIR spectroscopic studies," *Biochim. Biophys. Acta - Biomembr.*, vol. 1828, no. 2, pp. 213–222, 2013, doi: https://doi.org/10.1016/j.bbamem.2012.10.009.

[62] I. Budziak, M. Arczewska, and D. M. Kamiński, "Formation of Prenylated Chalcone Xanthohumol Cocrystals: Single Crystal X-ray Diffraction, Vibrational Spectroscopic Study Coupled with Multivariate Analysis," *Molecules* , vol. 24, no. 23. 2019, doi: 10.3390/molecules24234245.

[63] L. R. Chadwick *et al.*, "Estrogens and Congeners from Spent Hops (Humulus lupulus)," *J. Nat. Prod.*, vol. 67, no. 12, pp. 2024–2032, Dec. 2004, doi: 10.1021/np049783i.

[64] A. Lejardi, E. Meaurio, J. Fernández, and J.-R. Sarasua, "Miscibility of poly(vinyl alcohol)-graft-hydroxy ester/ poly(vinylpyrrolidone) blends," *Macromolecules*, vol. 44, no. 18, pp. 7351–7363, 2011, doi: 10.1021/ma2012305.

[65] C. Hou, T. Yang, X. Sun, Z. Ren, H. Li, and S. Yan, "Branched Crystalline Patterns of Poly(ε-caprolactone) and Poly(4-hydroxystyrene) Blends Thin Films," *J. Phys. Chem. B*, vol. 120, no. 1, pp. 222–230, Jan. 2016, doi: 10.1021/acs.jpcb.5b09960.

[66] R. Abreu-Villela, M. Schönenberger, I. Caraballo, and M. Kuentz, "Early stages of drug crystallization from amorphous solid dispersion via fractal analysis based on chemical imaging," *Eur. J. Pharm. Biopharm.*, vol. 133, pp. 122–130, Dec. 2018, doi: 10.1016/j.ejpb.2018.10.007.

[67] L. Jiang and J. Zhang, "6 - Biodegradable Polymers and Polymer Blends," in *Plastics Design Library*, S. B. T.-H. of B. and B. P. Ebnesajjad, Ed. Boston: William Andrew Publishing, 2013, pp. 109–128.

[68] C. C. Neikirk, J. W. Chung, and R. D. Priestley, "Thermomechanical behavior of hydrogen-bond based supramolecular poly(ε-caprolactone)-silica nanocomposites," *RSC Adv.*, vol. 3, no. 37, pp. 16686–16696, 2013, doi: 10.1039/C3RA42031K.

[69] I. Manavitehrani, A. Fathi, H. Badr, S. Daly, A. Negahi Shirazi, and F. Dehghani, "Biomedical Applications of Biodegradable Polyesters," *Polymers (Basel).*, vol. 8, no. 1, p. 20, Jan. 2016, doi: 10.3390/polym8010020.

[70] J. F. Stevens, A. W. Taylor, J. E. Clawson, and M. L. Deinzer, “Fate of xanthohumol and related prenylflavonoids from hops to beer,” *J. Agric. Food Chem.*, vol. 47, no. 6, pp. 2421–2428, Jun. 1999, doi: 10.1021/jf990101k.